Optics Letters

Multipulsing states management in all-normal dispersion fiber laser with a fiber-based spectral filter

Ankita Khanolkar[1] and Andy Chong[1,2,*]

[1]Department of Electro-Optics and Photonics, University of Dayton, Dayton, Ohio 45469, USA
[2]Department of Physics, University of Dayton, Dayton, Ohio 45469, USA
*Corresponding author: achong1@udayton.edu

Received 7 September 2020; revised 4 October 2020; accepted 13 October 2020; posted 14 October 2020 (Doc. ID 409339); published 19 November 2020

We report an experimental study of multipulsing states in an all-normal dispersion fiber laser using an all-fiber, tunable birefringent spectral filter. Various multipulsing states such as harmonic mode-locking and soliton bunches are observed by tuning the spectral filter. The multipulse evolution in this experiment relies only on the spectral filter characteristics, and it is independent of input pump power and saturable absorber effects. This laser provides an attractive option of controlling the pulse dynamics of a fiber laser with the use of a simple spectral filter.

https://doi.org/10.1364/OL.409339

Controlling the number of ultrafast pulses and the separation between them is important for various applications. For example, in optical communication, the digital communication bit rate depends on the proximity of individual pulses [1]. For instance, managing the burst of optical pulses is critical in improving the ablation rate in ultrafast micromachining, or producing electron bunches in an accelerator architecture. For such applications, multipulsing states of a mode-locked laser can be useful sources [2]. Multipulsing operations, which are related to soliton energy quantization, are studied theoretically as well as experimentally extensively [3–6]. In the case of all-normal dispersion (ANDi) fiber lasers, the pulses can be understood as the dissipative solitons in a normally dispersive medium with a gain and spectral filtering. These lasers can still generate multiple pulses due to pulse energy quantization [7]. The interaction between these pulses is of great interest, as they can lead to phenomena such as harmonic mode-locking, bound solitons, and soliton rains [8–13].

Soto-Crespo and Akhmediev showed that a structured shape of a spectral filter (SF) could lead to multipulse phenomena such as bound state solitons [14]. Komarov *et al.* theoretically demonstrated that the interaction between multiple pulses in an ANDi fiber laser can be controlled by introducing additional narrow spectral selection of intracavity radiation [15]. Haboucha *et al.* identified the spectral gain filtering as a mechanism of multiple pulse formation in passively mode-locked fiber lasers and proposed the idea of introducing an SF with a variable bandwidth (BW) in the cavity so as to generate multiple pulses [16]. Bao *et al.* implemented the idea of intracavity narrow spectral selection in the form of a dual filter to obtain soliton rains in an ANDi fiber laser. They also observed other multipulsing phenomena by varying multiple parameters such as input pump power and saturable absorber (SA) action, and by tuning the dual SF transmission. Hence, there was no clear demonstration that only an SF was responsible for all these multipulsing states. The laser had a maximum average output power of 13.28 mW with chirped pulse duration of 3.63 ps [12]. Huang *et al.* also used a dual SF in an all-fiber ANDi laser cavity with graphene oxide as an SA, but the formation of multiple pulses was always associated with simultaneous tuning of the pump power and SF transmission. The average output power of this laser was 0.19 mW, and with the repetition period of 933 ns, the overall energy was 0.2 nJ. The energy per pulse can be calculated to be lower than this, which is not useful for practical applications [13].

In this Letter, we experimentally verify the contribution of a single parameter, SF transmission, in multipulse generation in a mode-locked fiber laser by isolating the effects of other parameters such as pump power and SA. The birefringent fiber-based filter used in our experiments can yield a variety of transmission profiles, which eliminates the need for the dual filters used in [12,13]. Moreover, the performance of our laser is superior (~300 fs pulses with 300 mW average output power and >1 nJ energy per pulse) compared to previous research. Since the control of multipulsing states is convenient by adjusting the SF transmission, we believe our laser design will find its usage in a variety of applications that require burst mode operation of pulsed lasers.

The experimental configuration of the oscillator is similar to that in [17] and is shown in Fig. 1. A non-linear polarization evolution (NPE)-based SA in the form a polarization controller (PC1), half-wave plate (HWP), quarter-wave plate (QWP), and polarizing beam splitter (PBS) is employed to initiate the mode-locking process. The total length of the fibers in the cavity is 5.54 m, and the total cavity dispersion is 0.127 ps^2.

The SF in this laser cavity (shown in Fig. 2) consists of a section of single-mode fiber (SMF), polarization maintaining

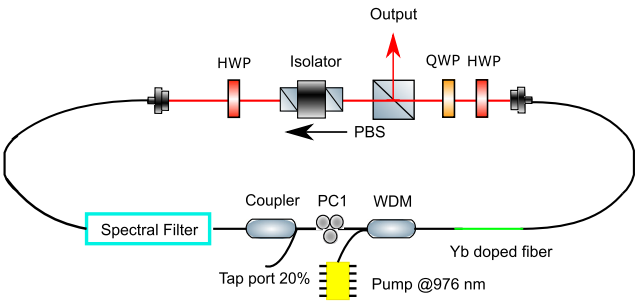

Fig. 1. Experimental setup of the fiber laser.

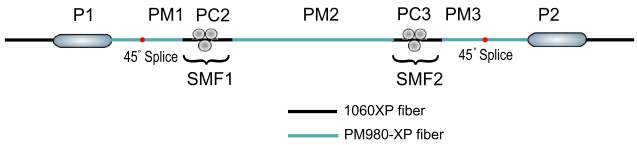

Fig. 2. Schematic of fiber-based spectral filter. P, polarizer; PC, polarization controller; PM, polarization maintaining fiber; SMF, single-mode fiber.

(PM) fiber, and another SMF (SMF1-PM2-SMF2) spliced between two PM fibers that are spliced to in-line polarizers at an angle of 45°. The PCs can be tuned to create a stress induced birefringence in the SMFs. This stress induced birefringence produces a polarization rotation that leads to a variety of transmission profiles. The transmission spectrum of the filter can be simulated using Jones calculus, and the transmittance is given by

$$T = P(\theta_2)\cdot W(\Delta\phi_5)\cdot R(-\Theta_2)\cdot W(\Delta\phi_4)\cdot R(\Theta_2)\cdot W(\Delta\phi_3)\cdot R(-\Theta_1)\cdot W(\Delta\phi_2)\cdot R(\Theta_1)\cdot W(\Delta\phi_1)\cdot P(\theta_1), \quad (1)$$

where $P(\theta)$ is the Jones matrix for the polarizer with the axis of transmission making an angle θ with the PM fibers (in this case, 45°). The Jones matrices for PM fibers and SMF are denoted by

$$W(\Delta\phi) = \begin{pmatrix} e^{-i\frac{\Delta\phi}{2}} & 0 \\ 0 & e^{i\frac{\Delta\phi}{2}} \end{pmatrix},$$

with $\Delta\phi_1$, $\Delta\phi_2$, $\Delta\phi_3$, $\Delta\phi_4$, and $\Delta\phi_5$ being the phase difference between light propagating between slow and fast axes PM1, SMF1, PM2, SMF2, and PM3, respectively. As SMFs are treated as rotated waveplates for this analysis, a rotator matrix $R(\Theta)$ has been used, where Θ_1 and Θ_2 are the angles of rotation of polarization inside the SMF1 and SMF2, respectively. Experimentally, by rotating or squeezing the PCs, the parameters $\Delta\phi_2$, $\Delta\phi_4$, Θ_1, and Θ_2 in Eq. (1) change and so does the transmission of the filter. A few sample simulated transmission spectra of the proposed SF are shown in Fig. 3. The lengths of the PM fibers in this filter are 10 cm, 25 cm, and 10 cm. The length of SMF sections is 14.5 cm each.

The transmission characteristics of the SF are experimentally observed by operating the laser cavity below lasing threshold at a very low pump power (50 mW). A broadband amplified spontaneous emission (ASE) [shown by a dashed curve in Fig. 4(a)] is coupled into the SF, and the filter output can be observed through the 20% port of the coupler. PC2 and PC3 are carefully

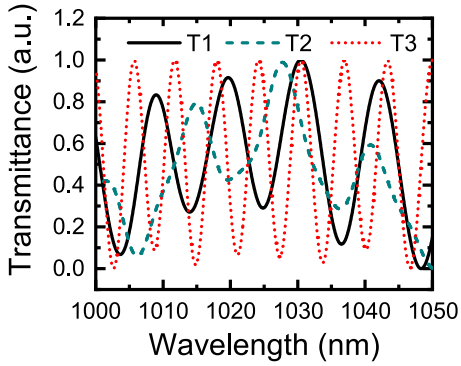

Fig. 3. Simulated transmission spectra of the filter. The calculated birefringence values for the PM fibers are $\Delta n_1 = \Delta n_3 = \Delta n_5 = 3.6 \times 10^{-4}$. Birefringence values for SMFs (Δn_2 and Δn_5) and rotation angles (Θ_1 and Θ_2) are variable.

tuned so that the output of the SF has a narrow BW, as suggested by Haboucha *et al.* [16]. The solid curve in Fig. 4(a) shows the filter output, while the inset shows the transmittance of the filter, and it closely follows the shape predicted by the simulation (curve T2 in the Fig. 3). Then, harmonic mode-locked operation (third harmonic) is achieved by rotating intracavity waveplates and tuning PC1 at a pump power of 650 mW. A high input pump power is used to facilitate observation of multipulsing [6]. A typical output spectrum ejected by the PBS is shown in Fig. 4(b). The optical spectrum taken at the 20% port of the fiber coupler [Fig. 4(c)] shows FWHM BW of 6.5 nm. The laser produces a stable pulse train [Fig. 4(d)] with 112 MHz repetition rate, which is measured by a 650 MHz oscilloscope together with a 1 GHz photodetector. To observe the pulse dynamics more carefully, we used a 6 GHz oscilloscope together with a 20 GHz photodetector, and the results are shown in Fig. 4(e). Figure 4(f) represents a radio frequency (RF) spectrum measured with a 500 MHz span and 1 kHz resolution BW. The main peaks occur at the pulse repetition rate (112 MHz), whereas smaller peaks are separated by the fundamental frequency of 37.5 MHz. The laser generates chirped pulses, which are dechirped to 290 fs duration with a grating pair outside the cavity [Fig. 4(g)]. The average mode-locked output power is 300 mW, which corresponds to an energy of 2.67 nJ per pulse.

From this mode-locked operation (Visualization 1) by gradually tuning PC3, the harmonic mode-locking slowly converts in a soliton bunch [Fig. 5(a)]. Now the laser mode-locks at the fundamental repetition rate of the cavity, i.e., 37.5 MHz, and the corresponding pulse train is shown in Fig. 5(b). Figures 5(c) and 5(d) show the RF spectrum with two different spans. Figures 5(e) and 5(f) show the subtle changes in the spectrum and 20% port output. Tuning PC3 not only changes the central wavelength of the filter transmission but also BW and the shape of the filter [shown in Fig. 5(g)], which leads to soliton bunch formation [14,16]. The inset shows the comparison between filter transmittance when the laser is harmonically mode-locked and when it is operating at the fundamental repetition rate. The average mode-locked power stays the same. As there is no significant difference in the spectral BW, the pulse duration is almost the same.

From this mode, the number of pulses in a bunch can be varied by tuning either PC2 or PC3 carefully, as shown in Visualization 2. Up to six pulses are obtained, as shown in

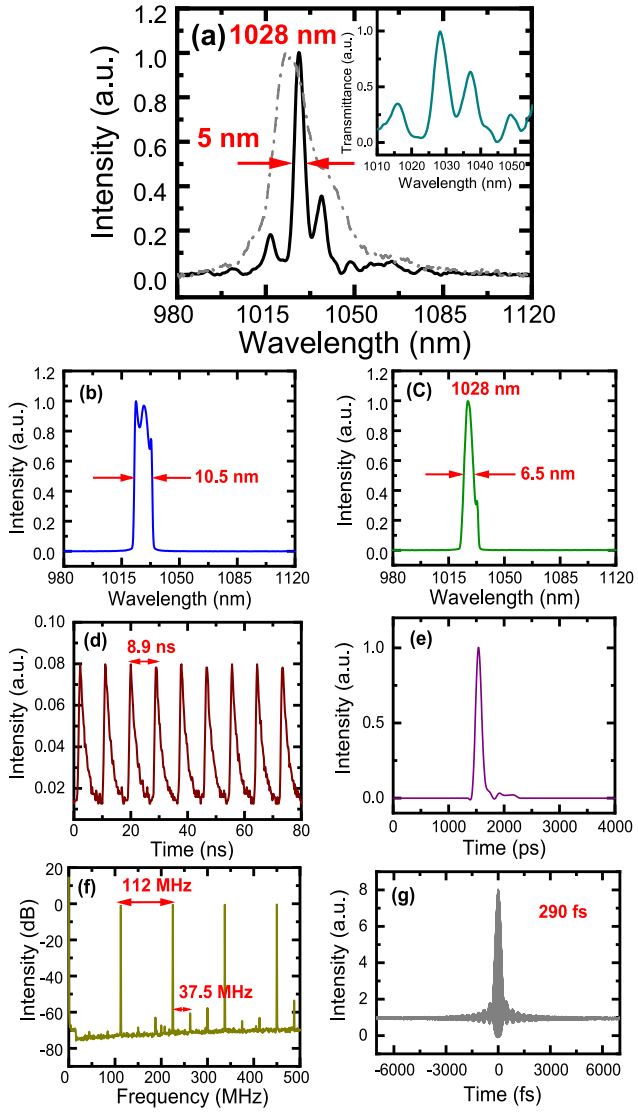

Fig. 4. Experimental data for the harmonic mode-locking (a) output spectrum of the SF with ASE (dashed line) as input. The inset shows experimental transmittance of the SF. (b) Mode-locked spectrum; (c) spectrum at the 20% port; (d) long range pulse train; (e) short range pulse train; (f) RF spectrum; span: 500 MHz, RBW: 1 kHz. (g) Autocorrelation.

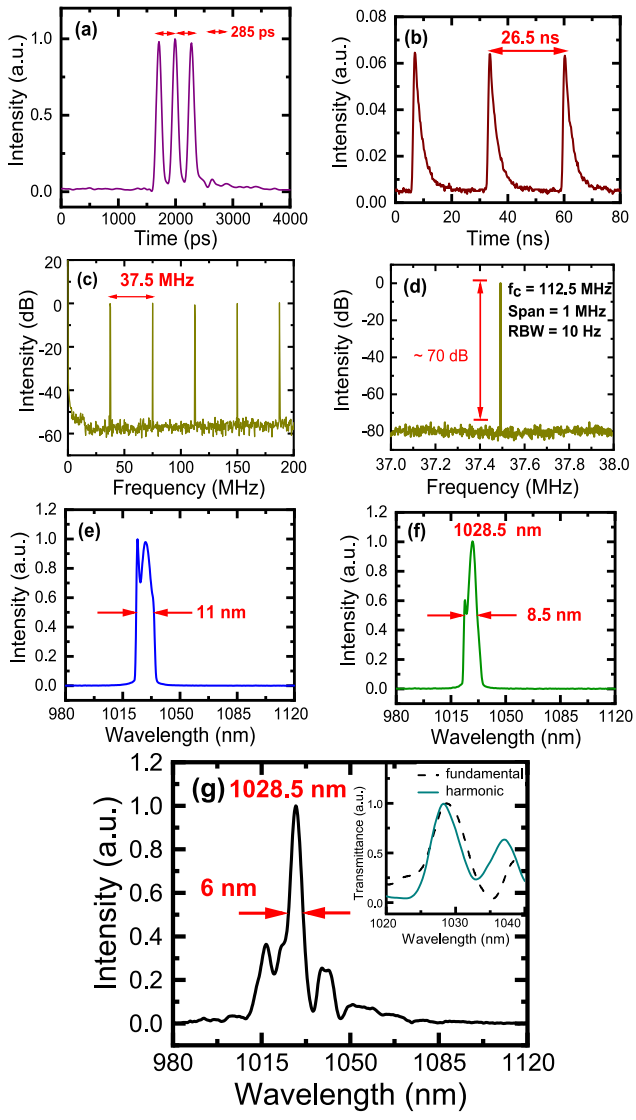

Fig. 5. Experimental data for the fundamental mode-locking (a) short range pulse train; (b) long range pulse train; (c) RF spectrum; span: 200 MHz, RBW: 1 kHz. (d) RF spectrum over 1 MHz span; (e) mode-locked spectrum; (f) spectrum at the 20% port; (g) output spectrum of the filter with ASE as input. Inset shows change in the transmittance of the filter.

Fig. 6(a), although the average output power and the repetition rate of the laser remain the same. The corresponding spectra, 20% port output, and shape of the SF are shown in Figs. 6(b), 6(c), and 6(d), respectively. For any modes, the pulses have a fixed separation value of ~285 ps. Figure 6(e) shows a clear difference in the shape of the filter transmittance as the number of pulses in the bunch is altered. Apart from the dissipative soliton bunch and harmonic mode-locking, other states can also be observed where multiple pulses exist in the cavity but the separation between them is not constant. The long range and short range pulse trains for such a non-periodic multipulsing state are shown in Figs. 7(a) and 7(b), respectively. The short range pulse train shows that each individual pulse can be a bunch of dissipative solitons. The corresponding spectrum, 20% output, SF output, and transmittance of the SF are shown in Figs. 7(c), 7(d), 7(e), and 7(f), respectively.

In conclusion, we have demonstrated multipulsing operation in an ANDi fiber laser using an all-fiber birefringent SF. By tuning the SF, a harmonically mode-locked state converts into a dissipative soliton bunch and vice versa. The multipulse evolution is clearly due to the change in transmission characteristics of the SF, especially the BW and the shape, as the laser is operated at a constant pump power and without any changes in the SA. We believe that the ability of this laser to produce energetic multiple pulses by controlling a single parameter in the laser cavity will make it useful for practical applications.

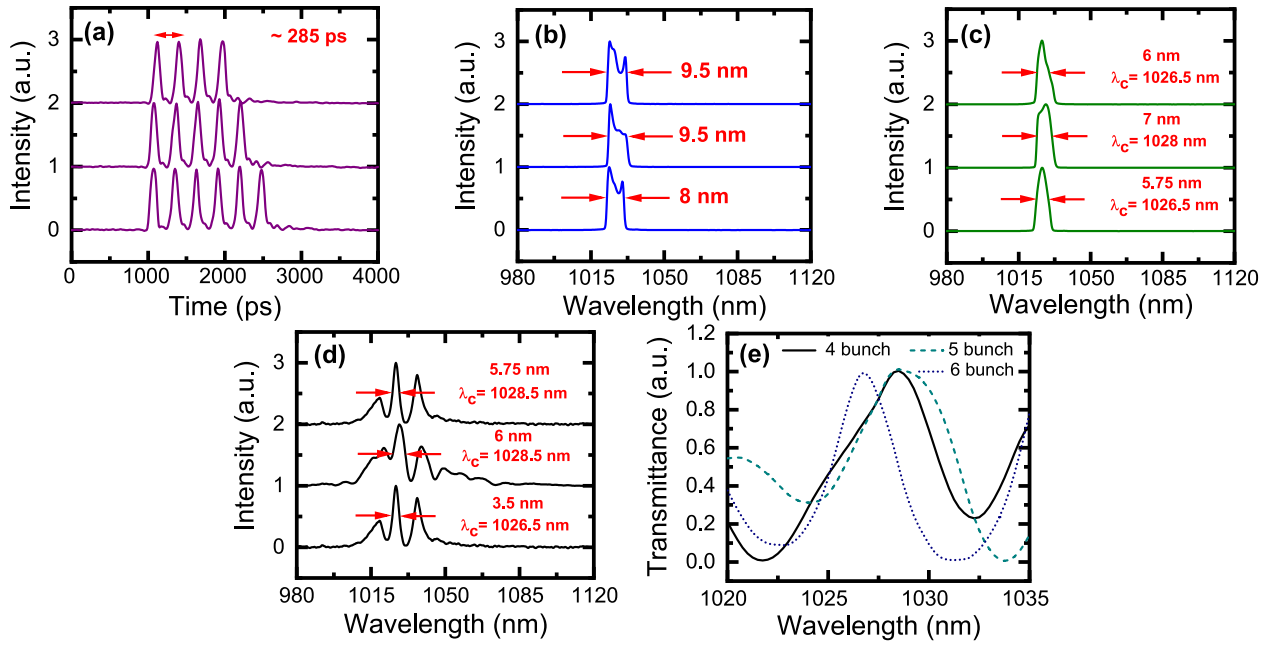

Fig. 6. Experimental data for the soliton bunch mode-locking (a) short range pulse train; (b) mode-locked spectrum at the PBS at 650 mW input power; (c) spectrum at 20% port; (d) SF output with ASE as input; (e) transmittance of the SF.

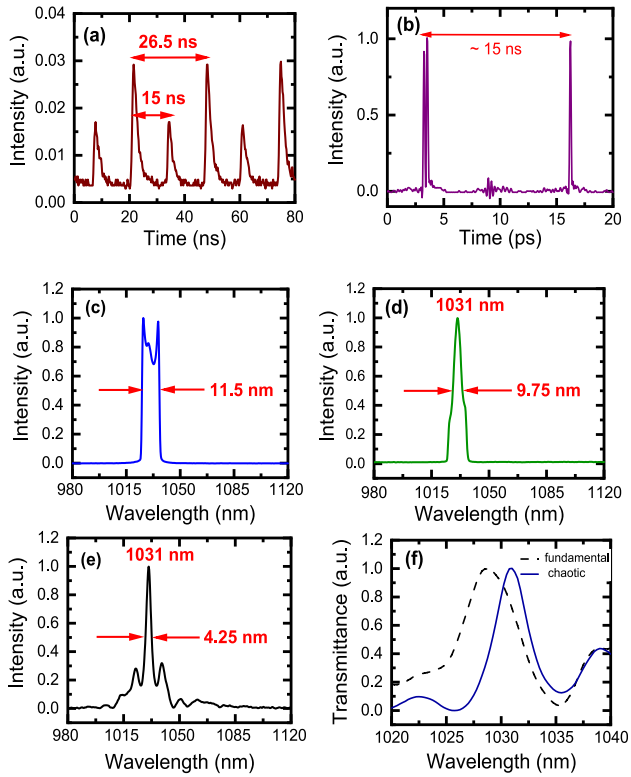

Fig. 7. Experimental data for the non-periodic mode-locked pulses (a) long range pulse train; (b) short range pulse train; (c) mode-locked spectrum; (d) spectrum at the 20% port; (e) output spectrum of the SF with ASE as input; (f) comparison of the SF transmittance.

Funding. NSF (EECS1710914).

Acknowledgment. The authors thank Monish Chatterjee and Julie Motz for lending the RF spectrum analyzer. The authors also thank Imad Agha for providing the 6 GHz oscilloscope.

Disclosures. The authors declare no conflicts of interest.

REFERENCES

1. N. Akhmediev and A. Ankiewicz, J. Nonlinear Sci. **10**, 600 (2000).
2. A. Mareczko, C. Vincent, A. Courjaud, C. Patrice, J.-L. Doualan, R. Moncorge, and E. Mottay, in *Advanced Solid State Lasers* (Optical Society of America, 2013), p. ATu3A–47.
3. A. Grudinin, D. Richardson, and D. Payne, Electron. Lett. **28**, 67 (1992).
4. D. Tang, W. Man, and H. Tam, Opt. Commun. **165**, 189 (1999).
5. B. Zhao, D. Tang, P. Shum, Y. Gong, C. Lu, W. Man, and H. Tam, Appl. Phys. B **77**, 585 (2003).
6. D. Tang, L.-M. Zhao, B. Zhao, and A. Liu, Phys. Rev. A **72**, 043816 (2005).
7. W. Renninger, A. Chong, and F. Wise, Phys. Rev. A **77**, 023814 (2008).
8. N. Akhmediev, J. M. Soto-Crespo, M. Grapinet, and P. Grelu, J. Nonlinear Opt. Phys. Mater. **14**, 177 (2005).
9. P. Grelu, F. Belhache, F. Gutty, and J. M. Soto-Crespo, J. Opt. Soc. Am. B **20**, 863 (2003).
10. B. Ortaç, A. Hideur, M. Brunel, C. Chédot, J. Limpert, A. Tünnermann, and F. Ilday, Opt. Express **14**, 6075 (2006).
11. J. Peng, L. Zhan, S. Luo, and Q. S. Shen, IEEE Photonics Technol. Lett. **25**, 948 (2013).
12. C. Bao, X. Xiao, and C. Yang, Opt. Lett. **38**, 1875 (2013).
13. S. Huang, Y. Wang, Y. Peiguang, G. Zhang, J. Zhao, H. Li, R. Lin, G. Cao, and J. Duan, Appl. Phys. B **116**, 939 (2014).
14. J. M. Soto-Crespo and N. Akhmediev, Phys. Rev. E **66**, 066610 (2002).
15. A. Komarov, K. Komarov, H. Leblond, and F. Sanchez, J. Opt. A **9**, 1149 (2007).
16. A. Haboucha, A. Komarov, H. Leblond, F. Sanchez, and G. Martel, Opt. Fiber Technol. **14**, 262 (2008).
17. A. Khanolkar, X. Ge, and A. Chong, Opt. Lett. **45**, 4555 (2020).